PIER C

(Received 23 January 2026, Accepted 5 March 2026, Scheduled 31 March 2026)

Printed Compact Monopole with Multiband Operation for Wi-Fi 8, 5G NR79, and 6G Upper Mid-Band Applications

Saou-Wen Su* and Guan-Lin Chen

Department of Computer and Communication Engineering
National Kaohsiung University of Science and Technology (NKUST), Kaohsiung 824005, Taiwan

ABSTRACT: A compact yet simple, printed monopole design targeted at providing multiband operation in the 2.4/5/6 GHz Wi-Fi 8 (2400–2484/5150–7125 MHz) bands and also the 5G new radio (NR79) (4.4–5.0 GHz) band and 6G upper mid-band in the 7.125–8.4 GHz range is demonstrated. The antenna is composed of longer and shorter radiating arms, as well as a matching stub that protrudes from the longer arm around the antenna port and extends toward the shorter arm. The two arms and the stub are all printed on a low-cost single-layer substrate. Four resonant modes of the antenna are excited, with the lower mode covering the 2.4 GHz band and the three upper modes forming a wide 7.4-dB return-loss bandwidth of about 4.3–8.6 GHz, covering the 5G NR79 band, 5/6 GHz Wi-Fi bands, and 6G upper mid-band. Additionally, the design can be fed by a commercially available coaxial cable, allowing the antenna to have considerable flexibility in installation within wireless devices.

1. INTRODUCTION

Monopole antenna was invented and patented by Guglielmo Marconi around 1895 [1] and is also known as the Marconi antenna. In practice, a monopole is made of a quarter-wavelength (0.25-λ) conductor mounted above an infinite ground with a 0.25-λ image in analysis, forming a 0.5-λ equivalent electric dipole [2]. The monopole antenna has been theoretically analyzed and widely used in mobile communications [2]. For compact and printed monopole antennas with a stand-alone design structure, several designs have been favorably studied and presented over the years [3–9]. These monopole designs include the use of folded monopole [4], hook-shaped radiating structures [3, 6, 7], branched monopole [5, 9], and the radiator loaded with multiple stubs [8]. Typically, these designs feature a main radiator and a relatively small signal ground for antenna feeding, together with an SMA coaxial connector or a coaxial cable feedline. In this case, the stand-alone structure allows the antenna to have more freedom when placed inside a wireless device, enabling it to attain an ideal transceiving location. However, among these stand-alone monopoles, the smallest antenna footprint, including signal ground, requires a minimum area of 200 mm^2 [4] to operate within the 2.4 GHz (2400–2484 MHz) and 5 GHz (5150–5825 MHz) frequencies only. In this paper, a new monopole design is introduced, which shows a similar design footprint and yet exhibits multiband/wideband properties for Wi-Fi 8 (IEEE 802.11bn) (2400–2484/5150–7125 MHz) operation [10, 11], the 5G new radio (NR) band 79 (4.4–5.0 GHz), and the future 6G upper mid-band (7.125–8.4) GHz range [12–14]. The Wi-Fi 8 operates within the same spectrum as Wi-Fi 7 but focuses on achieving ultra-high reliability (UHR) to enhance reliable communication [10, 11]. Commercialized Wi-Fi 8 devices are expected to be available in 2028 [11], while the initial rollout of the 6G network is anticipated in the 2028–2030 time frame [14]. Accordingly, multiband antennas capable of operating in the wireless heterogeneous networks [15–20], such as Wi-Fi 8 and 5/6G communications in this work, will be highly requested in the immediate future.

In this paper, we present a compact monopole design that can function in the heterogeneous networks of Wi-Fi 8 and 5G/6G communications. The antenna simply comprises a longer radiating arm, a shorter radiating arm, and a matching stub, all formed on a low-cost single-layer substrate. The overall design footprint is merely 7 mm $\times$ 30 mm, which corresponds to a 0.056- and 0.24-λ at 2.4 GHz in free space. Four resonant modes, namely modes 1, 2, 3, and 4, are excited, which are attributed to the fundamental and higher-order modes of the monopole and are controllable through parametric analyses. Mode 1 is responsible for operation in the 2.4 GHz band while modes 2, 3, and 4 form a very wide bandwidth of about 4.3–8.6 GHz to cover the 5G NR79 band, 5/6 GHz Wi-Fi bands, and 6G upper mid-band. Owing to the sizes of the two radiating arms not being far apart, the monopole design may be regarded as an asymmetric dipole in analysis. Thus, modes 1 (fundamental) and 2 (first higher order) can be determined by the combined length of the two arms. With the added matching stub that greatly assists better impedance for modes 3 and 4 (two higher-order modes), the proposed antenna is fully responsive for Wi-Fi 8 and 5/6G communications. Details of the design and its fabricated prototype are elucidated with numerical and measured results in the article.

* Corresponding author: Saou-Wen Su (saouwensu@nkust.edu.tw).

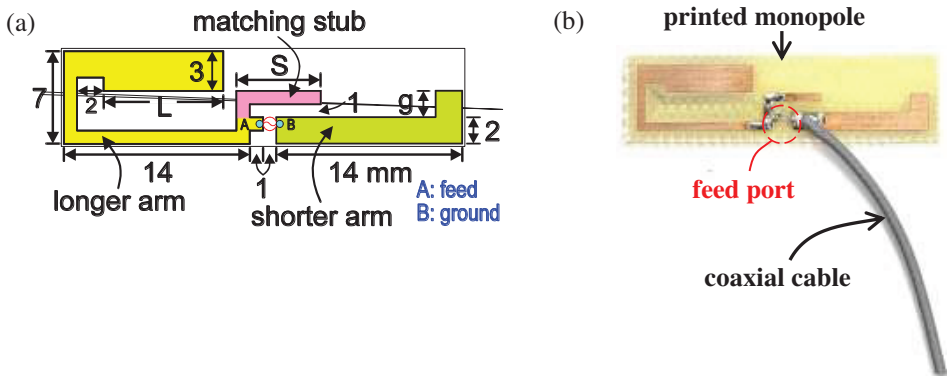

FIGURE 1. (a) Geometry of the printed compact monopole; $L = 9$ mm, $g = 2$ mm, $S = 6$ mm. (b) Photo of the prototype.

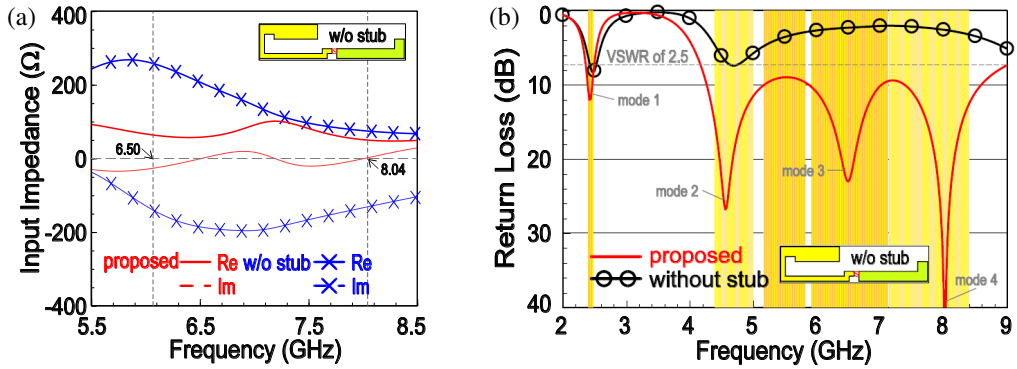

FIGURE 2. (a) Return losses and (b) input impedance for the proposed design and the case without the stub.

2. DESIGN CONSIDERATION

2.1. Monopole Configuration

Figure 1(a) shows the geometry of the proposed printed monopole antenna. The design is mainly composed of a longer radiating arm, a shorter radiating arm, and a matching stub, all formed on the same layer of a 0.8-mm-thick Flame Retardant 4 (FR4) substrate (relative permittivity 4.4 and loss tangent 0.024). The two arms are bent to reduce the overall antenna size with the dimensions 7 mm × 30 mm. The longer arm is connected to the signal at feed point A, while the shorter arm also serves as a small antenna ground that is further connected to the signal ground at point B. A clear view of the signal feeding can be seen in the photo in Fig. 1(b). The length of the monopole's longer arm can approximately be decided by using (1), where c is the speed of light in vacuum; f_0 is the fundamental frequency of the monopole; and ε_{eff} is the effective permittivity. The effective permittivity that makes the effective wavelength shorter is typically closer to 1 than 4.4 for the monopole with substantial fringing fields into the air.

$$l = \frac{c}{4f_0\sqrt{\varepsilon_{eff}}} \tag{1}$$

To achieve stable measurement results, a short 45-mm-long mini-coaxial cable with an overall diameter of 1.13 mm (O.D. 1.13) was employed. The feed gap between points A and B was set to 1 mm, with the center conductor of the cable soldered at point A and the outer copper at point B. Note that in this study, a tiny soldering pad of 1 mm × 1 mm was designed at point A to accommodate the center conductor of the cable feedline. In addition, to mitigate cable effects in the measurements, a snap-on ferrite choke close to the antenna feed port can be used to reduce unwanted cable currents, which can otherwise lead to radiation [21, 22].

Because both the radiating arms are comparable in size, the proposed monopole may be regarded as an asymmetric dipole formed by the two arms of unequal lengths [see the inset of the design without the stub in Fig. 2(a)]. In this case, the fundamental mode (mode 1) and the first higher-order mode (mode 2) can be determined by the overall combined length of the two radiating arms. Further, an L-shaped matching stub is added, protrudes from the longer arm around the antenna port, and extends along the shorter arm. In microwave engineering, the input impedance of the stub is reactive. In this design, the input impedance of the open stub is inductive, as shown in Fig. 2(b) for both cases with and without the stub. This stub helps compensate for the large capacitive reactance in the 5.5–8.5 GHz range to attain better impedance for the two higher-order modes (modes 3 and 4), as can be seen in Figs. 2(a) and (b). Modes 2, 3, and 4 can then form a wide bandwidth of about 4.3–8.6 GHz to include the 5G NR79 band, 5/6 GHz Wi-Fi bands, and 6G upper mid-band.

In this work, the proposed design generates four resonant modes at about 2.44, 4.58, 6.50, and 8.04 GHz. The associated surface-current distributions of each mode are presented in Fig. 3. At 2.44 GHz, high-intensity in-phase currents are dis-

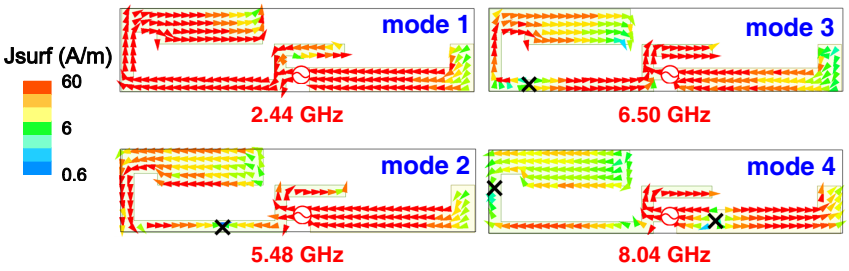

FIGURE 3. Current distributions for resonant modes at 2.44, 4.58, 6.50, and 8.04 GHz.

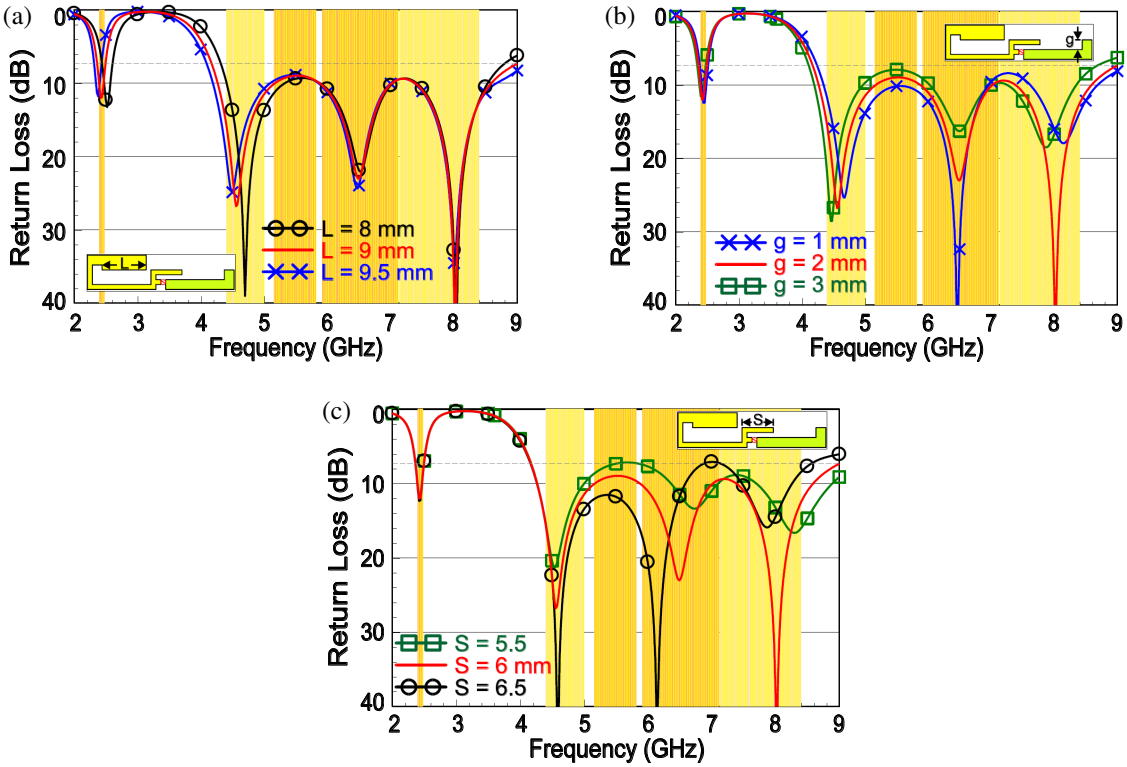

FIGURE 4. Return losses as a function of (a) arm length L, (b) ground length g, and (c) stub length S.

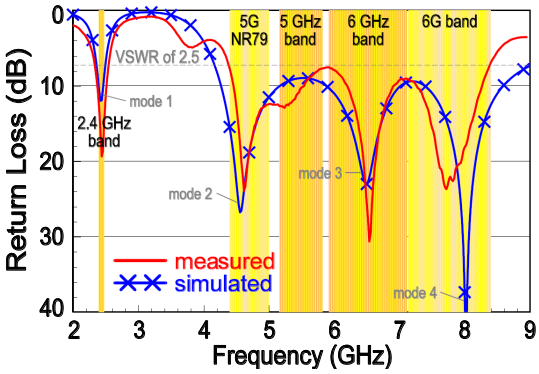

FIGURE 5. Simulated and measured return losses for the prototype studied in Fig. 1.

tributed along the longer and shorter arms, resembling a 0.5-λ dipole resonance in the 2.4 GHz band. At 4.58 GHz, a current null occurs on the longer arm in the 0.75-λ length while strong currents on the shorter arm correspond to the 0.25-λ resonant length. Accordingly, a 1.0-λ dipole-like resonance, by combining the two arms, is formed in the 5G NR79 band. In fact, the current distributions on the shorter arm are the same for both modes 1 and 2. The same properties can be applied to mode 3 at 6.5 GHz, at which one null is observed on the longer arm with similar antenna ground (shorter arm) currents. Finally, for higher-order mode 4 at 8.04 GHz, two nulls are further identified, reflecting the monopole design operating in a 1.5-λ dipole-like mode.

2.2. Parametric Studies

A range of parameters was examined using an electromagnetic (EM) simulator with the goal of showing the underlying causes of the antenna resonances. Fig. 4 presents a selection of results obtained from the EM analysis. The return losses as a function of arm length L are shown in Fig. 4(a). It is seen that this parameter significantly affects the first and second modes of the antenna as the length L varies. Longer length leads to decreased

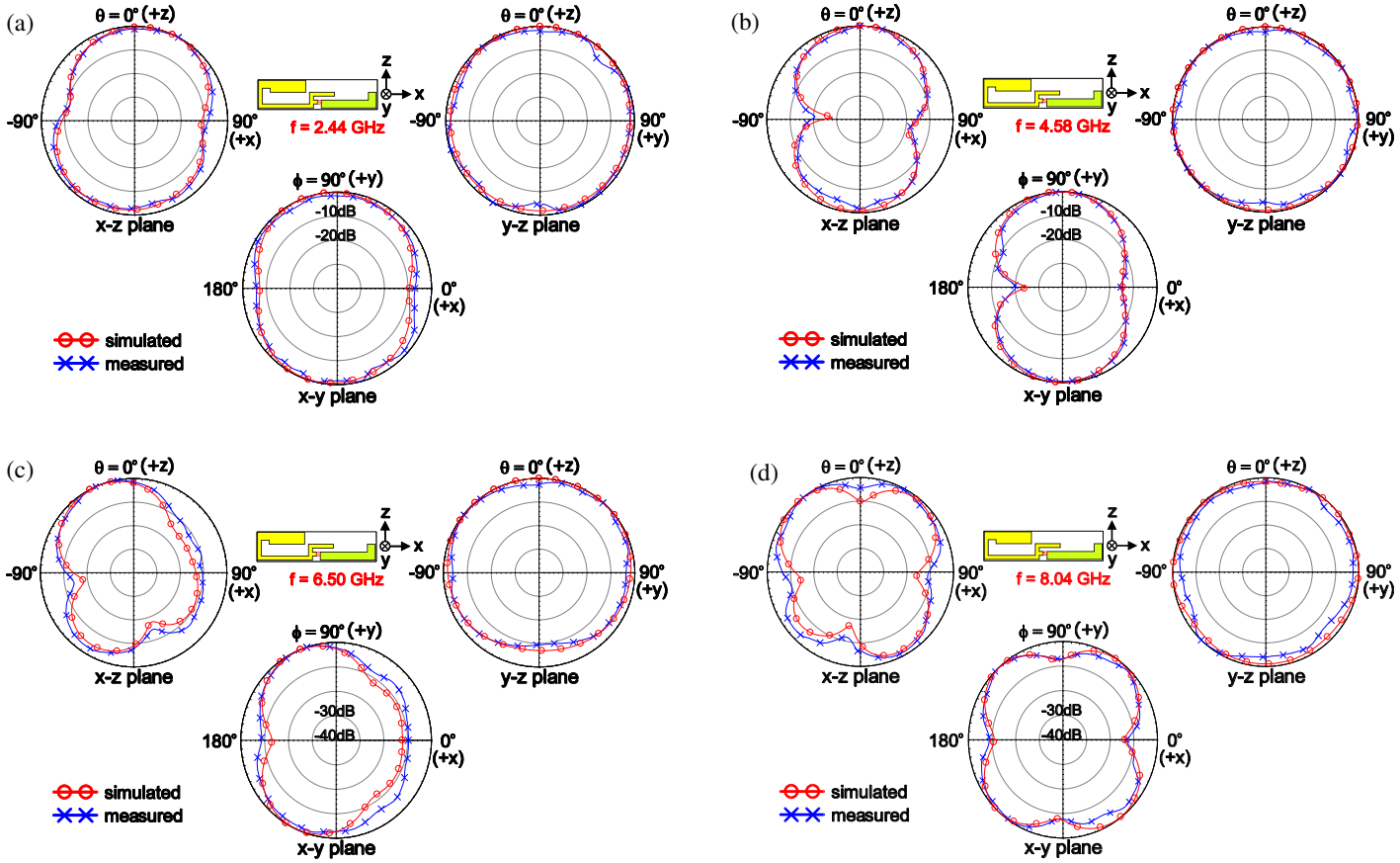

FIGURE 6. Simulated and measured 2-D radiation patterns at (a) 2.44, (b) 4.58, (c) 6.50, and (d) 8.06 GHz.

antenna frequencies for both modes 1 and 2. Fig. 4(b) shows the impact of ground length g, which has a relative effect on the frequencies of modes 2 and 4 in this design. With an increase in g, both modes 2 and 4 are shifted toward the lower frequencies, owing to an increased resonant length. Finally, in Fig. 4(c), the effects of stub length S on the return losses are primarily upon the third and fourth modes of the monopole in the 6–8.5 GHz range, with the frequencies of modes 1 and 2 unchanged. This is expected because the stub is added to offset the large capacitive reactance and improve impedance for modes 3 and 4. In general, one can first control mode 1 of the proposed design by adjusting arm length L, followed by ground length g for tuning modes 2 and 4, and lastly modes 3 and 4 by fine-tuning stub length S.

3. EXPERIMENTAL RESULT VERIFICATION

Figure 5 gives the return losses of the simulated and measured results for the prototype described in Fig. 1. It can be seen that the experimental data generally agree with the numerical results. The prototype covers all the 2.4/5/6 GHz Wi-Fi 8 bands, 5G NR79 band, and 6G upper mid-band range, which are also marked by five respective-colored bars. Within the bands of interest, the impedance matching all exceeds 7.4 dB return loss (voltage standing wave ratio (VSWR) of 2.5). The measured impedance bandwidth formed by the three upper modes is slightly narrower than the simulation and yet still covers the desired 4.4–8.4 GHz range. In addition, four resonant modes at approximately 2.44, 4.58, 6.50, and 8.04 GHz, corresponding to modes 1, 2, 3, and 4, are also identifiable. It is noteworthy that the 7.4 dB impedance is widely adopted for terminal-device antennas in industry and is also superior to the 6 dB criterion defined for several 5G mobile antennas reported in [23–28].

Figures 6(a)–(d) show the 2-D radiation patterns of antenna *E-total* fields at 2.44, 4.58, 6.50, and 8.04 GHz. In the fundamental mode at 2.44 GHz (mode 1), the design resembles an asymmetric dipole antenna placed along the $\pm x$ axial directions, with dipole-like radiation that exhibits an omnidirectional pattern in the y-z plane and radiation nulls along the x axis. For the first higher-order mode at 4.58 GHz (mode 2), similar radiation patterns to those obtained at 2.44 GHz in the y-z and x-y planes are observed. This is because the large end portion of the bent longer arm has an in-phase current flow with that on the shorter arm (see Fig. 3), resulting in the constructive far field along the $\pm y$ and $\pm z$ axial directions. For mode 3 at 6.5 GHz and higher-order mode 4 at 8.04 GHz, the radiation side lobes dominated by the out-of-phase currents on the longer and shorter arms become noticeable in the x-y and x-z planes.

The measured and simulated total efficiencies and realized gains are presented in Figs. 7(a) and (b). The measurements were made in an anechoic chamber by the ETS-Lindgren system using the great-circle method. The radiation efficiency was obtained by calculating the total radiated power from the antenna within a spherical region and dividing it by the 0 dBm input power provided to the antenna. The total efficiency takes

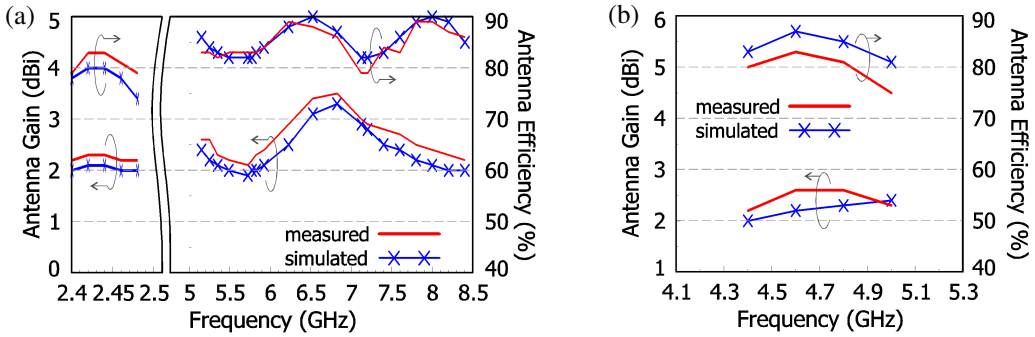

FIGURE 7. Simulated and measured total efficiencies and realized gains in the (a) 2.4/5/6 GHz bands and 6G upper mid-band and (b) 5G NR79 band.

TABLE 1. Comparison of the proposed design with cited works in [3–9].

Ref.	Bands (GHz)	Planar Size (λ)	Efficiency (%)	Peak Gain (dBi)	Feedline
[3]	2.4/5	0.08×0.21	N.A.	1.45 at 2.43 GHz 3.37 at 5.8 GHz	coaxial cable
[4]	2.4/5	0.06×0.20	N.A.	2.4 (2.4 GHz band) 4.5 (5 GHz band)	coaxial cable
[5]	2.4/5	0.16×0.20	N.A.	2 (2.4 GHz band) 3 (5 GHz band)	SMA
[6]	1.92–2.17 (UMTS) 2.4/5 2.5–2.69 (WiMAX)	0.13×0.13	N.A.	N.A.	SMA
[7]	2.4/5	0.14×0.15	N.A.	3.57*	SMA
[8]	2.4/5.8 3.4–3.8 (3.5 GHz band)	0.13×0.16	> 86 across all bands	2 at 2.45 GHz 2.1 at 3.5 GHz 2.5 at 5.8 GHz	SMA
[9]	2.4/5/6	0.05×0.15#	70 (2.4 GHz band) 67 (5/6 GHz bands)	2–2.8 (2.4 GHz band) 1.5–6 (5/6 GHz bands)	coaxial cable
Prop.	2.4/5/6 5G NR79 6G upper mid-band	0.05×0.24	79–83 (2.4 GHz band) 83–90 (5/6 GHz bands) 79–83 (5G NR79 band)	2.3 (2.4 GHz band) 2.2–3.5 (5/6 GHz bands) 2.4 (5G NR79 band)	coaxial cable

RL: Return Loss, λ is the free-space wavelength at the lowest designed frequency, N.A.: Not Available,
*Not specifying which band, #Not including antenna ground.

into account the antenna mismatch losses, and the mismatch factor is defined as $1 - |\Gamma|^2$, where Γ represents the voltage reflection coefficient [29]. The realized gain (or absolute gain), which also considers antenna mismatch losses, represents the peak E-total gain here in the measurements. In Fig. 7(a), the results in the 2.4 GHz band show that the peak gain is approximately 2.3 dBi, with a stable total efficiency of 79–83%. In the upper bands for 5/6 GHz operation and 6G upper-mid band (7125–8400 MHz), the gain ranges from 2.2 to 3.5 dBi, with the efficiency exceeding 83% and up to 90%. As for the 5G NR79 (4.4–5.0 GHz) band, the gain is approximately 2.4 dBi, and the efficiency is around 75–83%.

At the end, a comparison table, Table 1, is presented to compare the proposed design with cited works in [3–9]. Note that the thickness of the antenna substrate is neglected for simplicity. The proposed work covers most operating bands, including the Wi-Fi 2.4/5/6 GHz bands and 5G/6G bands for heterogeneous communications. In addition, the upper bands have the greatest fractional bandwidth of about 67% (bandwidth of 4.3 GHz over a center frequency of 6.45 GHz). Although the antenna size in [9] appears the smallest, the overall dimensions, including the antenna ground, reach 0.24-$\lambda \times$ 0.40-λ, as the monopole image ground can affect the antenna performance.

4. CONCLUSION

A small, printed monopole antenna supporting multiband operation for 2.4/5/6 GHz Wi-Fi 8, 5G NR79 (4.4–5.0 GHz), and the 6G upper mid-band (7.125–8.4 GHz) has been introduced and verified in this work. The antenna structure is simple, utilizing two asymmetrical radiating arms that are comparable in size and coupled with one matching stub for upper-band tuning. In this design, the width of 7 mm and length of 30 mm are relatively small, which correspond to a 0.056- and 0.24-λ at 2.4 GHz, respectively. The obtained four resonances, attributed to the fundamental and higher-order modes, can also be controlled through the antenna parametric analyses. In addition, the radiation patterns in the perpendicular plane (y-z cut

defined in this paper) to the antenna axial direction are stable across the desired operating bands. Over the 7.4 dB impedance bandwidth, the total efficiency is 79–83% in the lower band and 75–90% in the upper bands. The proposed work can be a strong candidate for consumer premise equipment in future heterogeneous communications.

REFERENCES

[1] IEEE, *"Inspiring Technology: 34 Breakthroughs" Celebrating 140 Years of Advancing Technology for the Benefit of Humanity*, 32–35, 2023.

[2] Balanis, C. A., *Antenna Theory: Analysis and Design*, John Wiley & Sons, 2016.

[3] Lee, C.-H. and S.-O. Park, "A compact printed hook-shaped monopole antenna for 2.4/5-GHz WLAN applications," *Microwave and Optical Technology Letters*, Vol. 48, No. 2, 327–329, 2006.

[4] Su, S.-W. and F.-S. Chang, "Compact, printed mobile-unit antenna for 2.4 and 5 GHz WLAN applications," *Microwave and Optical Technology Letters*, Vol. 52, No. 12, 2648–2653, 2010.

[5] Chen, W.-S., B.-Y. Lee, and P.-Y. Chang, "A compact and small printed monopole antenna for WLAN applications," *Microwave and Optical Technology Letters*, Vol. 53, No. 7, 1518–1522, 2011.

[6] Naser-Moghadasi, M., R. A. Sadeghzadeh, M. Fakheri, T. Aribi, T. Sedghi, and B. S. Virdee, "Miniature hook-shaped multiband antenna for mobile applications," *IEEE Antennas and Wireless Propagation Letters*, Vol. 11, 1096–1099, 2012.

[7] Yeo, W. L., K. C. Lai, K. H. Yeap, P. C. Teh, and H. Nisar, "A compact dual-band hook-shaped antenna for wireless applications," *Microwave and Optical Technology Letters*, Vol. 59, No. 8, 1882–1887, 2017.

[8] Fakhriddinovich, A. U., M. A. Sufian, W. A. Awan, N. Hussain, and N. Kim, "A compact antenna with multiple stubs for ISM, 5G sub-6-GHz, and WLAN," *IEEE Access*, Vol. 11, 130 418–130 425, 2023.

[9] Wi, S., H. Lee, J. Choi, J. Kim, R. Li, and H. Kim, "A compact dual-band antenna using a gap-coupled monopole branch for Wi-Fi 6/6E/7 applications," *Scientific Reports*, Vol. 16, 5331, 2026.

[10] Galati-Giordano, L., G. Geraci, M. Carrascosa, and B. Bellalta, "What will Wi-Fi 8 be? A primer on IEEE 802.11 bn ultra high reliability," *IEEE Communications Magazine*, Vol. 62, No. 8, 126–132, 2024.

[11] MediaTek, "Wi-Fi 8: Pioneering the future of connectivity," https://www.mediatek.com/tek-talk-blogs/wi-fi-8-pioneering-the-future-of-connectivity, 2024.

[12] Nokia Corporation, "6G mid-band spectrum technology explained," https://www.nokia.com/6g/6g-mid-band-spectrum-technology-explained/, 2024.

[13] Samsung Electronics Co., Ltd., "Upper mid-band spectrum for 6G: Opportunities and key enablers," https://research.samsung.com/blog/Upper-Mid-Band-Spectrum-for-6G-Opportunities-and-Key-Enablers#none, 2024.

[14] 5G Americas, "The 6G upgrade in the 7–8 GHz spectrum range: Coverage capacity and technology," https://www.5gamericas.org/wp-content/uploads/2024/10/The-6G-Upgrade-in-the-7-8-GHz-Spectrum-Id.pdf, 2024.

[15] Lee, C.-T., C.-C. Wan, and S.-W. Su, "Multi-laptop-antenna designs for 2.4/5/6 GHz WLAN and 5G NR77/78/79 operation," in *2020 International Symposium on Antennas and Propagation (ISAP)*, 421–422, Osaka, Japan, 2021.

[16] Yusuf, D. P., F.-H. Chu, and S.-W. Su, "Ultra-wideband Wi-Fi 6E/5G NR antenna for laptop applications," in *2022 Asia-Pacific Microwave Conference (APMC)*, 548–550, Yokohama, Japan, 2022.

[17] Su, S.-W. and Y.-L. Kuo, "Planar, metal-plate shorted monopole for Wi-Fi 7 and 6G applications," in *2024 International Symposium on Antennas and Propagation (ISAP)*, 1–2, Incheon, Korea, 2024.

[18] Su, S.-W., "Multiband, multimode, printed antenna for 5G, and Wi-Fi 7 laptop computer applications," *IEEE Access*, Vol. 13, 200 769–200 776, 2025.

[19] Su, S.-W., T.-C. Yu, and J.-C. Huang, "Flat-plate dipole antenna for Wi-Fi 8 and 6G operation," *Progress In Electromagnetics Research C*, Vol. 156, 201–205, 2025.

[20] Su, Y.-T. and S.-W. Su, "Low-cost, printed monopole antenna for Wi-Fi 8 and 6G laptop computers," in *2025 International Symposium on Antennas and Propagation (ISAP)*, 1–2, Fukuoka, Japan, 2025.

[21] DeMarinis, J., "The antenna cable as a source of error in EMI measurements," in *IEEE 1988 International Symposium on Electromagnetic Compatibility*, 9–14, Seattle, WA, USA, 1988.

[22] Hertel, T. W., "Cable-current effects of miniature UWB antennas," in *2005 IEEE Antennas and Propagation Society International Symposium*, 524–527, Washington, DC, USA, 2005.

[23] Sun, L., Y. Li, Z. Zhang, and H. Wang, "Self-decoupled MIMO antenna pair with shared radiator for 5G smartphones," *IEEE Transactions on Antennas and Propagation*, Vol. 68, No. 5, 3423–3432, 2020.

[24] Sim, C.-Y.-D., H.-Y. Liu, and C.-J. Huang, "Wideband MIMO antenna array design for future mobile devices operating in the 5G NR frequency bands n77/n78/n79 and LTE band 46," *IEEE Antennas and Wireless Propagation Letters*, Vol. 19, No. 1, 74–78, 2020.

[25] Chen, S.-C., L.-C. Chou, C.-I. G. Hsu, and S.-M. Li, "Compact sub-6-GHz four-element MIMO slot antenna system for 5G tablet devices," *IEEE Access*, Vol. 8, 154 652–154 662, 2020.

[26] Sun, L., Y. Li, and Z. Zhang, "Wideband decoupling of integrated slot antenna pairs for 5G smartphones," *IEEE Transactions on Antennas and Propagation*, Vol. 69, No. 4, 2386–2391, 2021.

[27] Sun, L., Y. Li, and Z. Zhang, "Wideband integrated quad-element MIMO antennas based on complementary antenna pairs for 5G smartphones," *IEEE Transactions on Antennas and Propagation*, Vol. 69, No. 8, 4466–4474, 2021.

[28] Wong, K.-L., C.-H. Shaw, W.-T. Li, and W.-Y. Li, "Ultra-wideband on-metal four-antenna module for 5G/6G/WiFi-6E IoT mobile device MIMO antennas and its field test study," *IEEE Access*, Vol. 12, 166 349–166 367, 2024.

[29] Balanis, C. A., *Antenna Theory: Analysis and Design*, John Wiley & Sons, 2016.